Proc. R. Soc. Lond. A **392**, 15–43 (1984)
Printed in Great Britain

Diabolical points in the spectra of triangles

BY M. V. BERRY, F.R.S., AND M. WILKINSON
H. H. Wills Physics Laboratory, University of Bristol, Tyndall Avenue, Bristol BS8 1TL, U.K.

(*Received* 27 *April* 1983)

'Accidental' degeneracies between energy levels E_j and E_{j+1} of a real Hamiltonian can occur generically in a family of Hamiltonians labelled by at least two parameters X, Y, ... Energy-level surfaces in E, X, Y space have (locally) a double-cone (diabolo) connection and we refer to the degeneracies themselves as 'diabolical points'. We studied the family of systems in which a particle moves freely within hard-walled triangles (vibrations of triangular membranes), with X and Y labelling two of the angles. Using an efficient Green-function technique to compute the levels, we found several diabolical points for low-lying levels (as well as some symmetry degeneracies); the lowest diabolical point occurred for levels 5 and 6 of the triangle 130.57°, 30.73°, 18.70°. The conical structure was confirmed by noting that the normal derivative u of the wavefunction ψ at a boundary point changed sign during a small circuit of the diabolical point. The form of the variation of u around a circuit, and the changing pattern of nodal lines of ψ, agreed with theoretical expectations. An estimate of the total number of degeneracies $\mathcal{N}_{\mathrm{d}}(j)$, involving levels 1 through j, based on the energy-scaling of cone angles and the level spacing distribution, gave $\mathcal{N}_{\mathrm{d}}(j) \sim (j+\frac{1}{2})^{2.5}$, and our limited data support this prediction. Analytical theory confirmed that for thin triangles (where our computational method is slow) there are no degeneracies in the energy range studied.

1. INTRODUCTION

Our purpose is to study degeneracies between discrete energy levels of quantal systems without symmetry and for which no magnetic fields are present, or, to put it more generally, between discrete eigenvalues of generic real Hermitian linear operators. For a single such system, degeneracies are infinitely unlikely and have traditionally been called 'accidental'. For a *family* of systems, however, it is possible to produce degeneracies by exploring the space of parameters X, Y, ... labelling members of the family. Von Neumann & Wigner (1929) showed that in general one parameter is insufficient to produce a degeneracy: at least two are required. Teller (1937) showed that the surfaces representing energy levels E in the space of E and the two parameters X, Y are connected at degeneracies like the two sheets of a double cone: a diabolo. To emphasize this conical geometry in the neighbourhood of degeneracies we shall refer to the connections as 'diabolical points'.

Diabolical points can occur in the electronic energy levels of a polyatomic molecule, which (in the adiabatic approximation) depend on parameters $X, Y, \ldots$ representing the configuration of nuclei. (Herzberg & Longuet-Higgins 1963; Desouter-Lecomte *et al.* 1979). As the molecule vibrates, and the nuclear configuration comes close to a diabolical point in the electron spectrum, an excited electron on the upper sheet of a cone can make a 'radiationless transition' to the lower sheet, in which the small energy difference is released not as a photon but into the nuclear vibrations. In a bold extension of this idea, Hill & Wheeler (1952) considered the energy levels of nucleons in a nucleus to depend parametrically on its external shape, and estimated the viscous resistance to change of shape by regarding radiationless transitions between diabolical points in the nucleon spectrum as the elementary acts of damping.

More recently, two aspects of the energy levels of semiclassical systems have been related to the existence of diabolical points in spectra of two-parameter families of generic Hamiltonians (Berry 1981, 1983*a*, *b*). The first aspect is the distribution $P(S)$ of the spacings S between neighbouring levels, previously considered (see, for example, Porter 1965) in the context of nuclear spectra. When S is small $P(S) \to 0$ as $S \to 0$ for generic systems, whose mechanics (classical or quantum) is non-separable in the coordinates. For separable systems by contrast, $P(S) \to$ constant as $S \to 0$ (Berry & Tabor 1977). The difference is attributable to the fact that separable systems exhibit the non-generic property that their levels can degenerate when just one parameter is varied. The second aspect is the presence of many 'avoided crossings' in curves of energy levels as functions of one parameter (Marcus 1980; Noid *et al.* 1980). Variation of just one parameter may cause the system to pass close to a diabolical point in the space augmented by a second parameter, and the avoided crossings are simply the approximately double-hyperbola curves obtained by slicing the diabolo near its vertex.

Only recently have a few diabolical points been exhibited by displaying conical structure in the energy levels of non-symmetrical systems depending on two or more parameters (in molecules; Vaz Pires *et al.* 1978; Dehareng *et al.* 1983). By contrast, there have been many studies of systems with geometric symmetry that can give rise to degeneracies whose nature can be understood in terms of group theory (see, for example, Knox & Gold 1964). We therefore choose to explore, in a systematic way, the spectrum of a non-symmetrical two-parameter family of systems whose levels can be determined fairly easily, with the intention of discovering diabolical points and determining some of their properties.

The family selected for study is *triangular quantum billiards*. These are two-dimensional systems with coordinates $\boldsymbol{r} = (x, y)$, whose eigenvalues k_j and eigenfunctions $\psi_j(\boldsymbol{r})$ are determined by solving the equation for the vibrations of triangular membranes, namely

$$\left.\begin{aligned} \nabla_{\boldsymbol{r}}^2 \psi_j(\boldsymbol{r}) + k_j^2 \psi_j(\boldsymbol{r}) = 0, \quad \boldsymbol{r} \text{ in B}, \\ \Psi_j(\boldsymbol{r}) = 0, \quad \boldsymbol{r} \text{ on } B, \end{aligned}\right\} \tag{1}$$

where B is a triangular boundary. B is specified by giving any two of the angles α, β, γ and the area $\mathscr{A}$. The dependence on $\mathscr{A}$ is a trivial scaling which we remove by defining the energy eigenvalues E_j in terms of the wavenumber eigenvalues k by

$$E_j = k_j^2/4\pi, \tag{2}$$

where the factor 4π is included to give the asymptotic energy levels an average spacing of unity (Baltes & Hilf 1976). Thus the space of triangles is effectively two-dimensional. The choice of triangle parameters X, Y (functions of α, β, γ) will be described in § 2.

To solve (1) an efficient computational scheme was employed, based on a Green-function technique which is explained in § 3. The resulting spectra $E_j(X, Y)$ are displayed in § 4. A number of diabolical points were found, and their energies and parameter values are listed in § 4 together with the corresponding values for degeneracies anticipated for reasons of symmetry in the equilateral and isosceles triangles.

In order to ensure that genuine degeneracies have been found (and not merely a close approach of blunted cones), we make use in § 5 of a remarkable topological result (Arnold 1978; Herzberg & Longuet-Higgins 1963; Longuet-Higgins 1975; Uhlenbeck 1976; Mead 1979, 1980, 1983; Mead & Truhlar 1979; Berry 1984): during a circuit of a diabolical point, each of the two wavefunctions changes sign. We confirm that such sign changes do occur, and also verify an analytical theory for the detailed form of the variation of wavefunctions when the circuits are small. We also display the interesting changes in the nodal pattern of the states around the circuits.

Computations for thin triangles are difficult, and to ensure that no diabolical points are missed when one or two angles are small an analytical theory is developed in § 6.

The density of diabolical points in E, X, Y space is expected to increase with E. In § 7 we estimate this effect by giving an approximate theory whose ingredients are the level spacing distribution $P(S)$ and the scaling with E of the cone angles.

2. Two-parameter space of triangles

Each triangle, with angles α, β, γ, can be represented by a point in the Euclidean space with cartesian coordinates α, β, γ. All such points lie in the equilateral triangle $\alpha+\beta+\gamma = \pi$ (figure 1). We remove the redundancy associated with labelling triangle vertices by defining $\alpha \geqslant \beta \geqslant \gamma$. Thus the essentially different triangles are represented by points in the 30°–60°–90° 'triangle of triangles' shown shaded in figure 1.

It is convenient to parametrize triangle space not by two angles but by variables X, Y defined as follows:

$$\left.\begin{aligned} \gamma &= 10Y, \\ \beta &= (1-\tfrac{1}{6}X)\,10Y + 10X, \end{aligned}\right\} \quad \gamma, \beta \text{ in degrees.} \tag{3}$$

This opens out the 'triangle of triangles' into the 'rectangle of triangles' $0 \leqslant X \leqslant 9$, $0 \leqslant Y \leqslant 6$. The rectangle is shown in figure 2, together with the contours of γ and β

and the locus of right triangles. The transformation from β, γ to X, Y is nonsingular except for the point $\gamma = \beta = 60°$ representing the equilateral triangle, which is spread out along the line $Y = 6$.

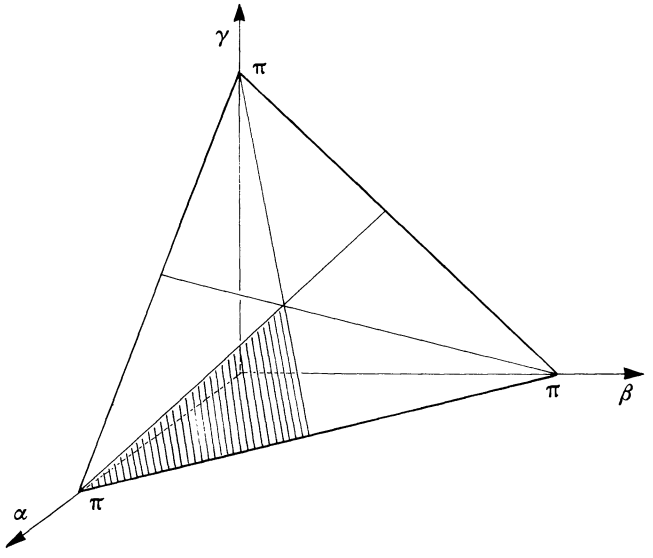

FIGURE 1. The 'triangle of triangles' (shaded) in the space of angles α, β, γ.

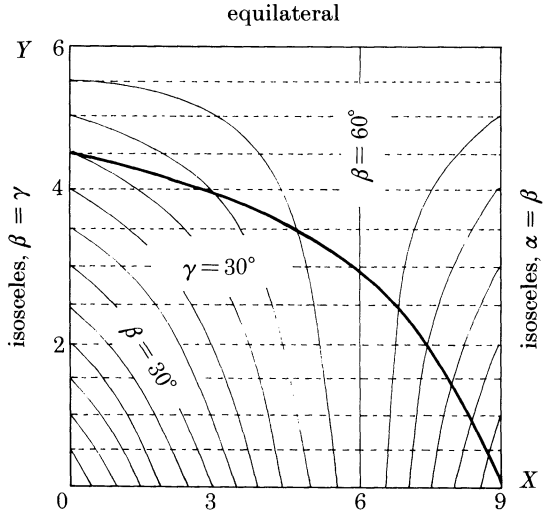

FIGURE 2. The 'rectangle of triangles' with parameters X, Y, showing contours of γ (dashed lines) $\leqslant \beta$ (full lines). The heavy line represents right triangles.

The only triangles for which the E_j and $\psi_j(\boldsymbol{r})$ have been determined analytically (Jung 1980) are 60°, 60°, 60°; 90°, 45°, 45°; 90°, 60°, 30°. For these triangles, the classical trajectories (geodesics in the triangle billiards) are integrable: in the four-dimensional phase space they explore two-dimensional tori, obtained by sewing

copies of the triangle corresponding to the finite number of directions which any single trajectory can adopt. For all three triangles, the spectra possess degeneracies to be described in § 4. Only the 90°, 60°, 30° triangle lies within, rather than on, the boundary of, the X, Y rectangle.

Of the remaining triangles, all except a set of measure zero have angles which are irrational multiples of π. Therefore typical trajectories explore infinitely many directions, so that these dynamical systems are non-integrable. It is an open question whether they are ergodic – that is, whether a typical trajectory explores almost all positions and directions – but it is known that trajectories in irrational triangles have zero entropy (Sinai 1976) and so cannot exhibit the exponential instabilities of fully chaotic systems such as the billiards of Sinai (1970) and Bunimovich (1974) (see Arnold 1978). Nevertheless, they do, as we shall see, appear to exhibit generic quantal behaviour so far as degeneracies and level spacings are concerned.

Triangles whose angles are rational multiples of π (and which form a set of measure zero) are classically *pseudointegrable* (Richens & Berry 1981), in the sense that their trajectories in phase space lie on two-dimensional surfaces that are, however, not tori (apart from the three special triangles already mentioned) but multiply-handled spheres (Zemlyakov & Katok 1975; Gutkin 1983). Quantally these too appear to exhibit generic behaviour.

Isosceles triangles form a special case, where the quantum states fall into two symmetry classes of even or odd parity with respect to the symmetry line. There is nothing preventing degeneracy between states with different symmetry, and so we expect, and shall find, degeneracies along the 'isosceles' lines $X = 0$ and $X = 9$ of the rectangle of triangles in figure 2.

3. Green-function formalism for calculating billiard spectra

To solve (1) we first reduce it to an integral equation round the boundary B. Let $\psi(\boldsymbol{r})$ be any solution of the differential equation in (1) with wavenumber k, and let $G(\boldsymbol{r}, \boldsymbol{r}')$ be the outgoing solution symmetric in $\boldsymbol{r}$ and $\boldsymbol{r}'$, of

$$\nabla_r^2 G(\boldsymbol{r}, \boldsymbol{r}') + k^2 G(\boldsymbol{r}, \boldsymbol{r}') = \delta(\boldsymbol{r} - \boldsymbol{r}'), \tag{4}$$

namely

$$G(\boldsymbol{r}, \boldsymbol{r}') = -\tfrac{1}{4}\mathrm{i} H_0^{(1)}(k|\boldsymbol{r} - \boldsymbol{r}'|), \tag{5}$$

where $H_0^{(1)}$ denotes the zero-order Hankel function of the first kind (Abramowitz & Stegun 1964). Multiplication of the G-equation by ψ and the ψ-equation by G, subtraction, integration over the area within B and use of Green's theorem give

$$\oint \mathrm{d}s' \{\psi(\boldsymbol{r}')\boldsymbol{n}' \cdot \nabla_{r'} G(\boldsymbol{r}, \boldsymbol{r}') - G(\boldsymbol{r}, \boldsymbol{r}')\boldsymbol{n}' \cdot \nabla_{r'} \psi(\boldsymbol{r}')\} = \begin{cases} \psi(\boldsymbol{r}), & \boldsymbol{r} \text{ within B}, \\ \tfrac{1}{2}\psi(\boldsymbol{r}), & \boldsymbol{r} \text{ on B}, \\ 0, & \boldsymbol{r} \text{ outside B}. \end{cases} \tag{6}$$

In this equation, s' is arc length round B, reckoned anticlockwise, and $\boldsymbol{n}'$ is the outward normal unit vector to B at $\boldsymbol{r}'$ (figure 3).

Define the normal component of the gradient of ψ at s on B by

$$u(s) \equiv \boldsymbol{n}\cdot\nabla_r\psi(\boldsymbol{r}(s)), \tag{7}$$

then a nonsingular integral equation for $u(s)$ can be obtained by taking the normal derivative of (6) with $\boldsymbol{r}$ lying on B, and by using the boundary condition that $\psi = 0$ on B. Thus

$$u(s) = -2\oint \mathrm{d}s' u(s')\,\boldsymbol{n}\cdot\nabla_r G(\boldsymbol{r},\boldsymbol{r}'). \tag{8}$$

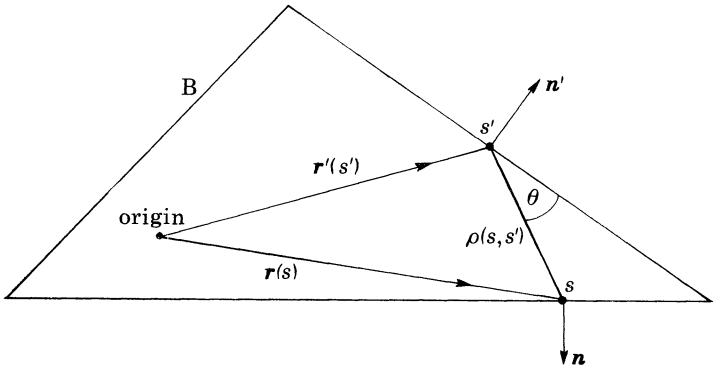

FIGURE 3. Notation for geometry associated with chord of triangle boundary B.

Next, we define $$\rho(s,s') = |\boldsymbol{r}(s)-\boldsymbol{r}(s')| \tag{9}$$

as the length of chord between s and s', and let $\theta(s,s')$ be the angle between the chord and the tangent to B at s (figure 3). Then use of (5) together with

$$\boldsymbol{n}\cdot\nabla_r G = \sin\theta(s,s')\,\partial G/\partial\rho \tag{10}$$

gives, finally $$u(s) = -\tfrac{1}{2}\mathrm{i}k\oint \mathrm{d}s' u(s')\sin\theta(s,s')\,H_1^{(1)}\{k\rho(s,s')\}. \tag{11}$$

(In appendix A we show that u satisfies a normalization condition (A 13) involving k.)

To obtain a scheme for computing the wavenumbers k from this linear homogeneous integral equation, it is desirable to employ a discrete representation for $u(s)$. A mathematically obvious choice is the Fourier coefficients of u with respect to s, which is a cyclic coordinate whose period $\mathscr{L}$ is the length of the perimeter of B,

and for many purposes this may be computationally efficient too. In our computations, however, it turned out to be more economical to simply discretize the boundary by dividing it into K segments. Defining

$$s_m \equiv ml/K, \quad \rho(s_l, s_m) \equiv \rho_{lm}, \quad \theta(s_l, s_m) \equiv \theta_{lm}, \quad 1 \leqslant (l, m) \leqslant K, \tag{12}$$

equation (11) gives the consistency condition for the energy levels E (defined in terms of k by (2)) as

$$\Delta(E; X, Y) = 0, \tag{13}$$

where

$$\Delta = \lim_{K\to\infty} \det M \tag{14}$$

and M denotes the $K \times K$ matrix whose elements are

$$M_{lm} \equiv \delta_{lm} + (\mathrm{i}k\mathscr{L}/2K) \sin\theta_{lm} H_1^{(1)}(k\rho_{lm}). \tag{15}$$

This is a non-Hermitian complex matrix in which k (or E) occurs nonlinearly. the billiard geometry is embodied in θ_{lm} and ρ_{lm} which thus depend on the parameters X, Y. Before embarking on computations of Δ as a function of E whose real zeros are the eigenvalues of the Hermitian operator defined by (1), it is necessary to check two aspects of the formalism.

Firstly, the limit in (14) must make sense. To see that it does, we expand Δ in terms of traces of powers of $M - 1$, using

$$\Delta = \lim_{K\to\infty} \exp\{\mathrm{tr} \ln M\} = \lim_{K\to\infty} \exp\left\{-\sum_{n=1}^{\infty} \frac{(-1)^n}{n} \mathrm{tr}\,(M-1)^n\right\}. \tag{16}$$

From (15),

$$\lim_{K\to\infty} \mathrm{tr}\,(M-1)^n = \lim_{K\to\infty} (\mathrm{i}k\mathscr{L}/2K)^n \sum_{l_1} \sum_{l_2} \cdots \sum_{l_n} \prod_{j=1}^{n} \sin\theta_{l_j l_{j+1}} H_1^{(1)}(k\rho_{l_j l_{j+1}}). \tag{17}$$

But, symbolically,

$$\lim_{K\to\infty} \frac{\mathscr{L}}{K} \sum_{l_j} = \oint \mathrm{d}s_j, \tag{18a}$$

so that

$$\lim_{K\to\infty} \mathrm{tr}\,(M-1)^n = (\tfrac{1}{2}\mathrm{i}k)^n \oint_{(s_{n+1}=s_1)} \mathrm{d}s_1 \cdots \oint \mathrm{d}s_n \prod_{j=1}^{n} \sin\theta(s_j, s_{j+1}) H_1^{(1)}\{k\rho(s_j, s_{j+1})\}. \tag{18b}$$

This shows that Δ can be represented exactly in terms of integrals over n-chord closed cycles of B. The representation is very convenient for analytical purposes, and resembles the formalism employed by Balian & Bloch (1972) to study semiclassical oscillations in the level density, but we will not pursue this aspect here.

Secondly, we must confirm that M (15) is nonsingular in spite of the presence of the Hankel function which diverges as ρ^{-1} as $\rho \to 0$. If s_l and s_m lie on the same side of the triangle, $\sin\theta_{lm}$ is identically zero and the corresponding element M_{lm} is identically δ_{lm}. But if s_l and s_m lie on different sides and close to the same corner, then ρ_{lm} can vanish without $\sin\theta_{lm}$ vanishing, and these elements of M_{lm} can be very large. However, the normal derivative $u(s)$ vanishes as s approaches a corner s_0; if the corner has angle α, it can be shown by the methods of § 6 that

$u \sim |s-s_0|^{(\pi/\alpha-1)}$, and this is sufficient to ensure convergence of the boundary integral in (11) in the limit $K \to \infty$. Nevertheless, the large matrix elements near corners do cause Δ to converge slowly for thin triangles, and this led us to supplement the numerical calculations by developing the analytical theory of § 6.

In practical computation it is of course not possible to take the limit $K \to \infty$. To estimate how large K must be in order to obtain a close approximation to an eigenvalue k, we note that k corresponds to a de Broglie wavelength $\lambda \equiv 2\pi/k$ and realize that this is the smallest scale on which waves $\psi(r)$ and their normal derivatives $u(s)$ may vary. It is therefore necessary to sample B at least several times (say t) in each de Broglie wavelength, giving

$$K_{\min} = t\mathscr{L}/\lambda = (t/2\pi)\, k\mathscr{L}. \tag{19}$$

For the most accurate computations (near diabolical points) it was necessary to take $t \approx 8$, which led to matrices of order $K \approx 125$ for the highest states studied.

As E varies through an isolated eigenvalue E_j (for fixed X, Y), the determinant behaves like

$$\Delta(E) = (E-E_j)\,\Delta'(E_j) + \ldots . \tag{20}$$

This implies that in the Argand plane, with coordinates $\mathrm{Re}\,\Delta$ and $\mathrm{Im}\,\Delta$, Δ passes smoothly through the origin as E passes E_j. This is the behaviour for generic X, Y. We are interested, however, in the behaviour near diabolical points, that is near double zeros of Δ. At a diabolical point, Δ has a double zero E^*, and

$$\Delta(E) = \tfrac{1}{2}(E-E^*)^2\,\Delta''(E^*) + \tfrac{1}{6}(E-E^*)^3\,\Delta'''(E^*), \tag{21}$$

This shows that Δ passes through a cusp at the origin as E passes E^*. Explicitly, by orienting axes in the Δ-plane so that $\mathrm{Re}\,\Delta''(E^*) = 0$, (21) gives

$$\mathrm{Re}\,\Delta = \tfrac{1}{6}\mathrm{Re}\,\Delta'''(E^*)\,(2/\mathrm{Im}\,\Delta''(E^*))^{\frac{3}{2}}\,(\mathrm{Im}\,\Delta)^{\frac{3}{2}}. \tag{22}$$

As the triangle is deformed to make X, Y vary through a diabolical point at X^*, Y^*, the Argand variation of Δ with E consists of a loop (crossing the origin twice at the two nearby eigenvalues) that shrinks to a cusp and then expands again. These types of behaviour are illustrated in figure 4 with a computed example.

For large K, the zeros E_j of Δ will not be purely real but will possess small imaginary parts whose values indicate the accuracy of the truncation. The reality of the zeros could be preserved by employing a real (standing-wave) Green function, involving the Neumann function $Y_0(k|\boldsymbol{r}-\boldsymbol{r}'|)$ instead of (5). This would lead to a matrix resembling (15) but with real elements, but has the disadvantage that the determinant analogous to Δ possesses numerous 'false' zeros E which are not solutions of the eigenvalue problem, in addition to those that are. The false zeros could sometimes be diagnosed by the fact that they possess parabolic coalescences rather than conical crossings, but there were many cases to which this diagnosis was not applicable and so we chose to eliminate this nuisance altogether by working with a complex Δ.

Finally, we point out that the formalism developed in this section is by no means

restricted to triangular, or even polygonal, boundaries, and applies equally to smoothly curved quantum billiards. Similar techniques have been developed by De Mey (1976), Niwa *et al.* (1980), Riddell (1979) and Tai & Shaw (1974), and applied to the calculation of low-lying levels.

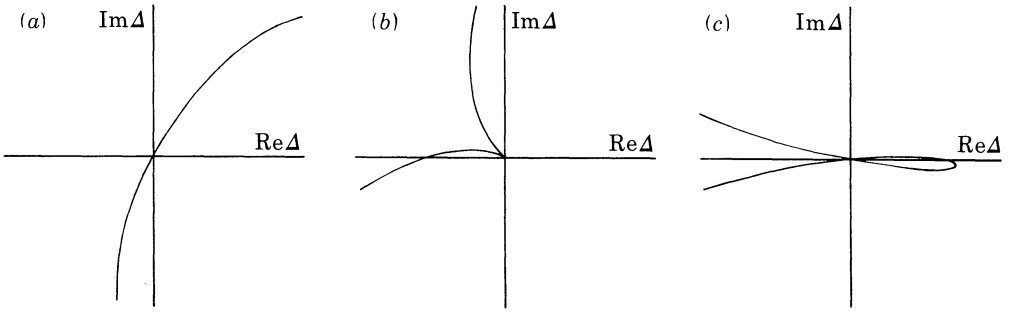

FIGURE 4. Variation of the complex determinant $\Delta(E; X, Y)$ with E, for the triangle $X = 4.61$, $Y = 3.97$ (cf. figure 6). (*a*) E passing through level 8, which is non-degenerate; (*b*) E passing through the degeneracy of levels 6 and 7; (*c*) E passing through levels 9 and 10 which are almost degenerate.

4. Distribution of diabolical points

For points X, Y in the rectangle of triangles, the complex determinant Δ ((14) and (15)) was computed as a function of E, and its zeros in the range $(0 < E < 18)$ were determined; these are the energy levels of the triangle X, Y. This procedure was carried out for the grid of triangles in which X ranged from 0 to 9 in steps of unity, and Y ranged from 0.6 to 6 in steps of 0.2. For each value of X, the data were plotted as curves of $E_j(Y)$. A typical set of levels (for $X = 7$) is shown as the thick lines in figure 5. There are many avoided crossings, suggesting the presence of diabolical points elsewhere in the X, Y plane. To find them, a finer grid of triangles was examined in each region where the diabolical points were thought to lie, and the precise location of the points was determined by iteration with Newton's method. The existence of each degeneracy was tested by calculating the two relevant eigenfunctions on an X–Y circuit enclosing it, and seeing whether they changed sign (this test will be described in more detail in § 5).

Twelve diabolical points were found in this way; their parameters and energies are listed in table 1. The lowest diabolical point occurs between levels 5 and 6, for an obtuse triangle. One might call this the 'paradoxical triangle', because it is the generic triangle with the special property that no other triangle (other than symmetric ones) has a lower pair of degenerate levels. It is possible to check that the angles are not close to low-order rational multiples of π by expanding them into continued fractions. This gives $\beta \sim 7\pi/41$ and $\gamma \sim 8\pi/77$, to the accuracy of table 1, and is strong evidence that the triangle is nonspecial.

The next diabolical point occurs between levels 6 and 7, for an acute triangle whose angles are well approximated by $\alpha \sim 93\pi/197$ and $\gamma \sim 55\pi/179$; again, these

are reassuringly far from low-order rationals. Figure 6 shows $E_j(Y)$ for the value $X = 4.61$ corresponding to a slice through this diabolical point. The near-crossing of levels 9 and 10 in figure 6 reflects the proximity of the next diabolical point, at $X = 4.85$, $Y = 4.06$.

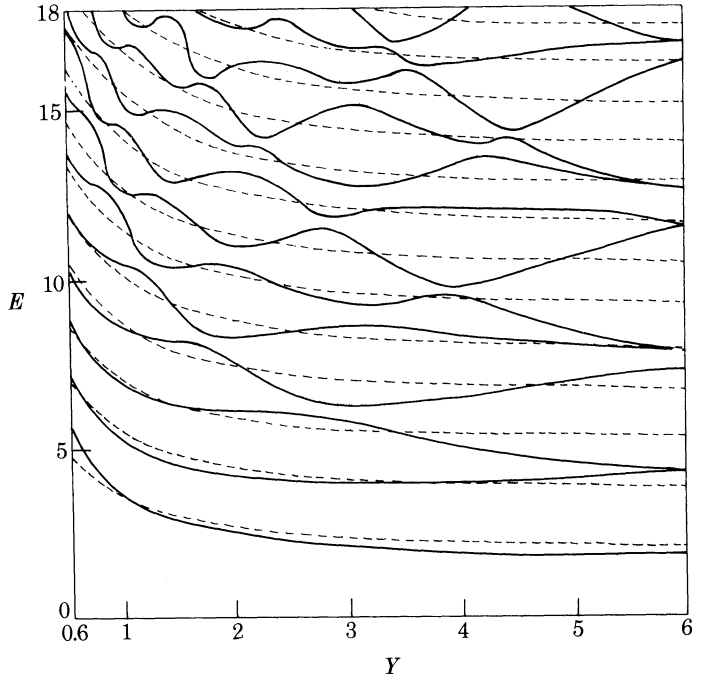

FIGURE 5. Energy level curves for $E_j(Y)$ (full lines) for $X = 7$, showing avoided crossings. The dashed lines are smoothed energy level curves $E_j^{sm}(Y)$, calculated from (28).

Also listed on table 1 are the symmetry degeneracies between states of even and odd parity for isosceles triangles. These are illustrated by figure 7*a*, which shows $E_j(Y)$ for $X = 9$, corresponding (figure 2) to triangles with their two larger angles equal. The crossings are evidently actual, rather than avoided as in figures 5 and 6. Two of the isosceles degeneracies in table 1 lie very close to the line $Y = 6$, and are resolved by magnification in figures 7*b* and *c*.

The last group of entries in table 1 is the list of degeneracies of the equilateral triangle $Y = 6$, which can be seen on the right-hand sides of figures 5, 6 and 7*a*. All the levels (not just the degenerate ones) are known exactly. They are given by the formula (Richens & Berry 1981).

$$E_{mn} = (\pi/3\sqrt{3})(m^2+n^2-mn), \quad 1 \leqslant m \leqslant \tfrac{1}{2}n. \tag{23}$$

States with $n = 2m$ are non-degenerate; all the others are degenerate with multiplicity two because of symmetry. (This does not mean that the *levels* have these multiplicities; indeed Pinsky (1980) shows that the asymptotic levels have increasing

TABLE 1. DEGENERACIES IN TRIANGLE SPECTRA

levels	E	X	Y	α/deg	β/deg	γ/deg
			diabolical points			
5, 6	10.02	1.75	1.87	130.57	30.73	18.70
6, 7	9.79	4.61	3.97	84.98	55.30	39.72
7, 8	14.44	2.38	1.02	139.88	29.94	10.18
8, 9	14.27	2.85	1.53	128.16	36.55	15.29
8, 9	16.67	0.94	1.00	152.06	17.90	10.04
9, 10	13.74	4.85	4.06	83.10	56.29	40.61
9, 10	16.42	2.94	1.16	133.10	35.30	11.60
9, 10	16.35	0.86	1.51	143.35	21.53	15.12
10, 11	16.74	3.20	1.70	123.11	39.94	16.95
11, 12	16.06	5.20	3.88	84.01	57.19	38.80
11, 12	17.44	2.03	2.26	122.12	35.25	22.63
12, 13	17.43	5.53	3.37	89.15	57.16	33.69
			isosceles degeneracies			
4, 5	7.85	0	3.12	117.64	31.18	31.18
6, 7	12.15	0	1.83	143.32	18.34	18.34
7, 8	14.47	0	1.51	149.80	15.10	15.10
8, 9	12.86	0	3.45	111.04	34.48	34.48
8, 9	14.22	0	2.20	136.00	22.00	22.00
8, 9	16.67	0	1.28	154.34	12.83	12.83
11, 12	15.73	0	4.65	87.04	46.48	46.48
11, 12	16.2	0	3.8	104.00	38.00	38.00
11, 12	16.89	0	3.07	118.62	30.69	30.69
3, 4	6.07	9	2.81	75.97	75.97	28.06
4, 5	8.17	9	1.77	81.14	81.14	17.72
5, 6	7.88	9	5.77	61.15	61.15	57.70
5, 6	8.87	9	3.19	74.03	74.03	31.94
5, 6	10.34	9	1.28	83.59	83.59	12.82
6, 7	10.65	9	2.01	79.95	79.95	20.10
6, 7	12.55	9	1.00	85.02	85.02	9.96
7, 8	12.63	9	1.45	82.78	82.78	14.44
7, 8	14.76	9	0.81	85.93	85.93	8.14
8, 9	12.31	9	3.40	73.01	73.01	33.98
8, 9	13.21	9	2.39	78.03	78.03	23.94
8, 9	13.59	9	2.17	79.18	79.18	21.64
8, 9	14.76	9	1.18	84.42	84.42	11.16
8, 9	16.92	9	0.69	86.58	86.58	6.84
9, 10	15.32	9	1.55	82.23	82.23	15.54
9, 10	16.83	9	0.91	85.47	85.47	9.06
10, 11	14.13	9	4.45	67.77	67.77	44.46
10, 11	17.22	9	1.20	83.99	83.99	12.02
11, 12	16.22	9	3.46	72.73	72.73	34.54
11, 12	16.50	9	2.83	75.87	75.87	28.26
11, 12	16.98	9	2.27	78.66	78.66	22.68
12, 13	16.60	9	3.62	71.90	71.90	36.20
12, 13	16.95	9	5.89	60.58	60.58	58.84
			equilateral degeneracies			
2, 3	4.23		6	60	60	60
5, 6	7.86		6	60	60	60
7, 8	11.49		6	60	60	60
9, 10	12.70		6	60	60	60
12, 13	16.93		6	60	60	60

multiplicities, for number-theoretic reasons not obviously connected with symmetry.)

Similarly, the energy levels of the other two special triangles are known exactly, and give useful confirmation of the accuracy of the computations. For the 45°, 45°, 90° triangle ($X = 0$, $Y = 4.5$)

$$E_{mn} = \tfrac{1}{8}\pi(m^2+n^2), \quad 1 \leqslant m < n. \tag{24}$$

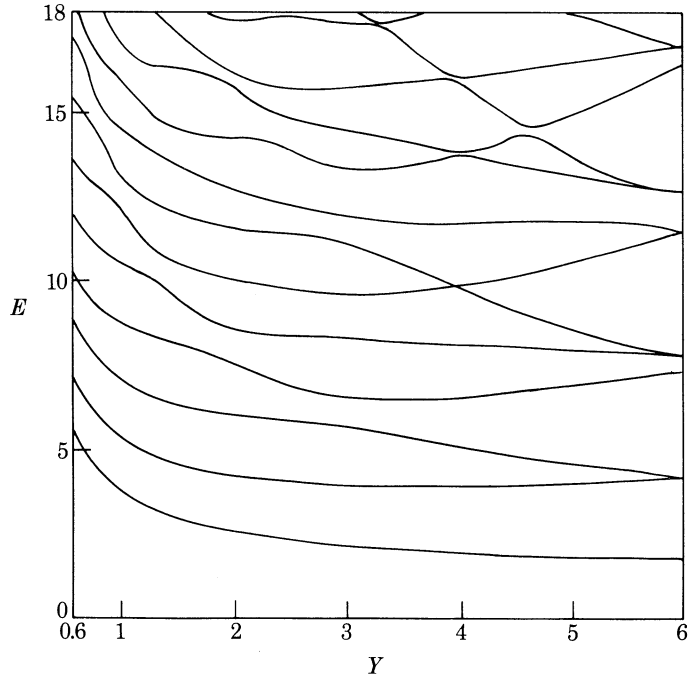

FIGURE 6. Energy level curves $E_j(Y)$ for $X = 4.61$ showing a crossing (slice through a diabolical point) of levels 6 and 7 at $Y = 3.97$, and a near-crossing of levels 9 and 10 at $Y = 4.02$.

All states are non-degenerate, but the levels show number-theoretic degeneracies which for large E dominate the spectrum (Berry 1981); the first occurs for levels 19 and 20, at $E = 25.53$, by virtue of the fact that $7^2+4^2 = 8^2+1^2$. For the 30°, 60°, 90° triangle ($X = 6$, $Y = 3$), the states are the odd-parity subset of the equilateral states (23), and

$$E_{mn} = (\pi/6\sqrt{3})(m^2+n^2-mn), \quad 1 \leqslant m < \tfrac{1}{2}n. \tag{25}$$

All states are non-degenerate, but the levels show number-theoretic degeneracies; the first occurs for levels 20 and 21 at $E = 27.51$, because

$$10^2+1^2-10\times 1 = 11^2+5^2-11\times 5.$$

The form of the energy surfaces $E_j(X, Y)$ 'on the average', that is with the degeneracies removed and the surfaces locally smoothed in X and Y, can be

explained in terms of a theory for the *mode number* $\mathcal{N}(E)$, defined as the number of levels with energies less than E, namely.

$$\mathcal{N}(E) \equiv \sum_{j=1}^{\infty} \Theta(E-E_j), \quad \text{where} \quad \Theta(x) = \begin{cases} 0 (x < 0), \\ \frac{1}{2} (x = 0), \\ 1 (x > 0). \end{cases} \tag{26}$$

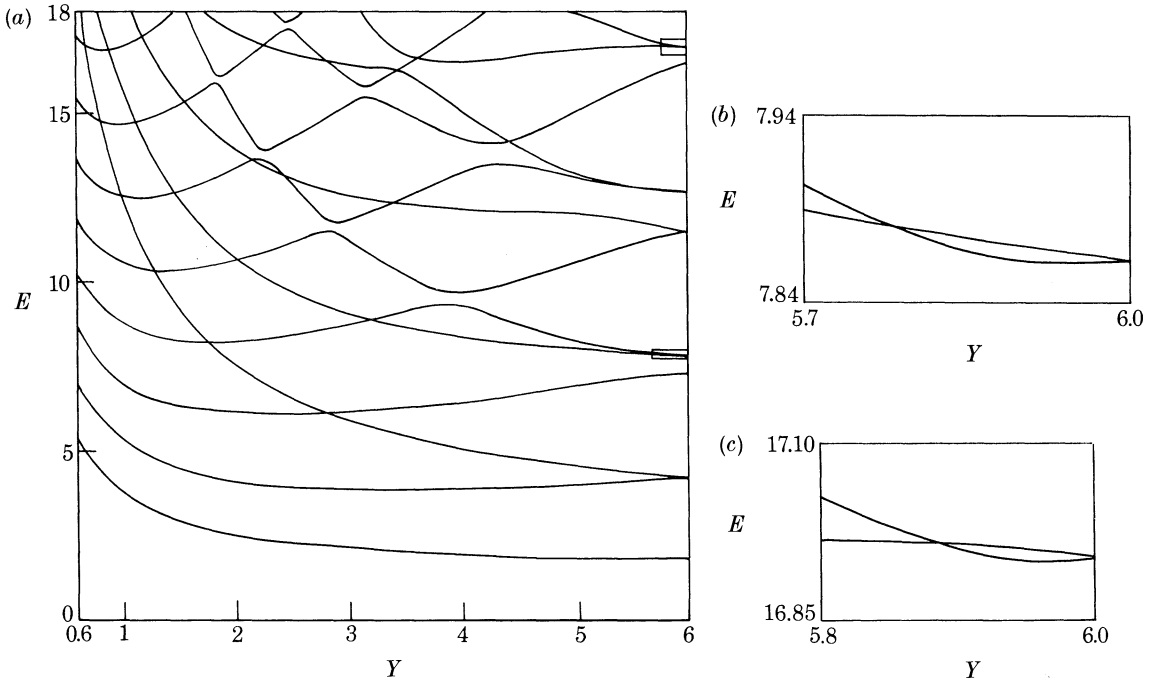

FIGURE 7. (*a*) Energy level curves $E_j(Y)$ for $X = 9$ (corresponding to isosceles triangles with their larger angles equal), showing crossings of states with different parity. (*b*) and (*c*) magnifications of the small boxes in (*a*), which show isosceles degeneracies very close to equilateral ones.

Baltes & Hilf (1976) review asymptotic formulae in which the stepped function $\mathcal{N}(E)$ is approximated smoothly in a series of falling powers of E. When applied to triangles, these formulae give $\mathcal{N} \sim \mathcal{N}^{sm}$, where

$$\mathcal{N}^{sm}(E) = E - \tfrac{1}{2}[\mathscr{L}E^{\frac{1}{2}}/(\mathscr{A}\pi)^{\frac{1}{2}}] + \tfrac{1}{24}(\pi/\alpha + \pi/\beta + \pi/\gamma - 1) + O(E^{-r}), \tag{27}$$

where $\mathscr{L}$ and $\mathscr{A}$ are the perimeter and area of the triangle, and $r > 0$.

According to (26), the jth level can be approximated by setting $\mathcal{N}^{sm}(E)$ equal to $j - \frac{1}{2}$. On using (27), we obtain the levels E_j^{sm}:

$$E_j^{sm} = j' + \tfrac{1}{2}Q^2 + \tfrac{1}{2}Q(Q^2 + 4j')^{\frac{1}{2}}, \tag{28}$$

where

$$j' = j - \tfrac{11}{24} - \tfrac{1}{24}\pi(1/\alpha + 1/\beta + 1/\gamma),$$

and

$$Q \equiv \frac{\sin\alpha + \sin\beta + \sin\gamma}{(2\pi \sin\alpha \sin\beta \sin\gamma)^{\frac{1}{2}}}. \tag{29}$$

The predictions of this formula are shown for $X = 7$ as the fine lines in figure 5. Two things are clear from the way the true levels $E_j(Y)$ oscillate across the smoothed levels $E_j^{sm}(Y)$: the formula (28) is a very accurate approximation (even for the ground state, which is surprising in an asymptotic theory); and the computations have not missed any levels.

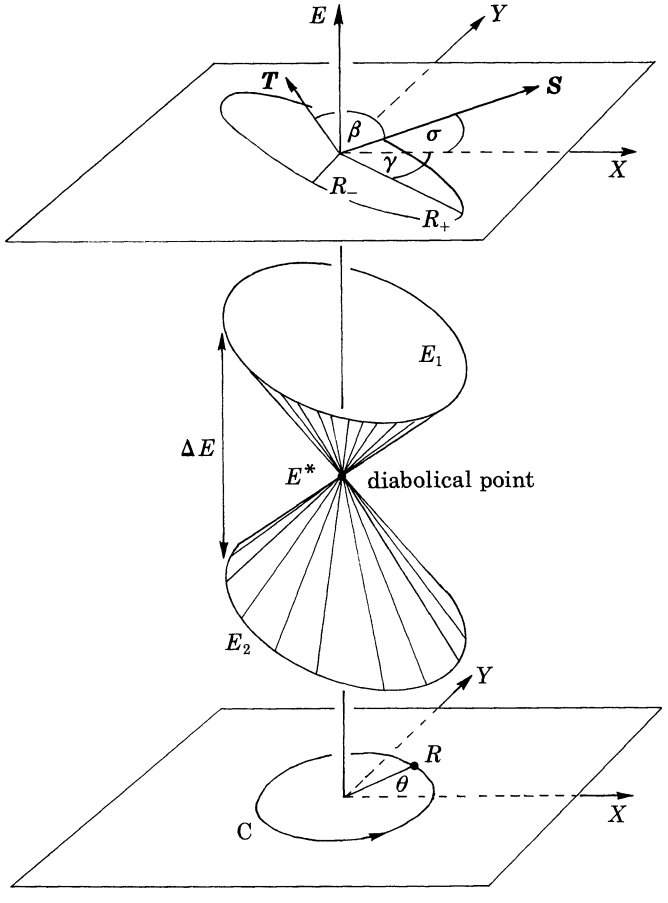

FIGURE 8. Geometry and notation near a diabolical point.

5. SMALL CIRCUITS OF DIABOLICAL POINTS

Referring to figure 8, we consider a diabolical point at energy E^* and triangle parameters X^*, Y^* which we take for simplicity to lie at the origin of X–Y space. If the Hamiltonian operator is $\hat{H}(X, Y)$, the two degenerate states $|\psi_1^*\rangle$ and $|\psi_2^*\rangle$ satisfy

$$\hat{H}(0,0)\,|\psi_1^*\rangle = E^*\,|\psi_1^*\rangle, \quad \hat{H}(0,0)\,|\psi_2^*\rangle = E^*\,|\psi_2^*\rangle. \tag{30}$$

Near the diabolical points, the geometry of the energy surfaces $E_1(X, Y)$ and $E_2(X, Y)$, and the nature of the states $|\psi_1\rangle$ and $|\psi_2\rangle$, are determined by the matrix elements

$$H'_{ij}(X, Y) \equiv \langle\psi_i^*|\,\hat{H}(X, Y) - \hat{H}(0,0)\,|\psi_j^*\rangle, \quad i,j = 1,2. \tag{31}$$

Degenerate perturbation theory (Teller 1937) gives the energies as

$$E_{1,2} = E^* + \tfrac{1}{2}[H'_{11} + H'_{22} \pm \{(H'_{11} - H'_{22})^2 + 4H'^2_{12}\}^{\frac{1}{2}}]. \tag{32}$$

The conical structure follows from this, together with the fact that the H'_{ij} vary linearly near $X = Y = 0$. In § 7 and appendix A we shall describe in detail how the H'_{ij} depend on the triangle deformations. For the present it is sufficient to represent the matrix elements in terms of two vectors $\boldsymbol{T}$ and $\boldsymbol{S}$ in $\boldsymbol{R} \equiv (X, Y)$ space (figure 8), defined by

$$\left.\begin{aligned} H'_{11} - H'_{22} &\equiv \boldsymbol{T}\cdot\boldsymbol{R}, \\ 2H'_{12} &\equiv \boldsymbol{S}\cdot\boldsymbol{R}. \end{aligned}\right\} \tag{33}$$

Thus
$$\Delta E \equiv E_1 - E_2 = \{(\boldsymbol{T}\cdot\boldsymbol{R})^2 + (\boldsymbol{S}\cdot\boldsymbol{R})^2\}^{\frac{1}{2}}. \tag{34}$$

Let $\boldsymbol{S}$ and $\boldsymbol{T}$ have lengths S and T and make angles σ and τ with the X direction, and let

$$\boldsymbol{S}\cdot\boldsymbol{T} \equiv ST\cos\beta, \quad S/T \equiv V. \tag{35}$$

Then β and V determine the cone geometry as follows. For level separation ΔE, the major and minor radii $R_\pm$ of the elliptic cone sections (projected onto the X–Y plane) are given by

$$1/R_\pm^2 = [T^2/2(\Delta E)^2]\,(1 + V^2 \mp \{1 + V^4 + 2V^2\cos 2\beta\}^{\frac{1}{2}}), \tag{36}$$

which shows that circular cones correspond to $V = 1$ and $\beta = \frac{1}{2}\pi$ and highly eccentric cones to $V \ll 1$ or $V \gg 1$. The angle γ made by the major axis with the X direction is

$$\gamma = \tfrac{1}{2}\arccos\left[\frac{-V^2\cos 2\sigma - \cos 2\tau}{(V^4 + 1 + 2V^2\cos^2\beta)^{\frac{1}{2}}}\right]. \tag{37}$$

We remark (with Arnold 1978) that the conical geometry near a diabolical point closely resembles that near an umbilic point of a surface (Berry & Hannay 1977; Berry & Upstill 1980) at which the two principal curvatures are equal. However, the 'surface' (considered as a deviation from the X–Y plane) whose curvature difference would be equal to $\Delta E(X, Y)$ exists only locally, and cannot be continued in any obvious way to include degeneracies between more than one pair of levels.

The states $|\psi_1\rangle$ and $|\psi_2\rangle$ are linear combinations of $|\psi_1^*\rangle$ and $|\psi_2^*\rangle$, which we write in terms of a 'mixing angle' $\chi(X, Y)$ as

$$|\psi_j\rangle = \cos\chi_j(X, Y)\,|\psi_1^*\rangle + \sin\chi_j(X, Y)\,|\psi_2^*\rangle, \quad j = 1, 2. \tag{38}$$

Degenerate perturbation theory (Berry 1981), together with (33), gives

$$\mathrm{e}^{2\mathrm{i}\chi_{1,2}} = \pm\,(\boldsymbol{T}\cdot\boldsymbol{R} + \mathrm{i}\boldsymbol{S}\cdot\boldsymbol{R})/[(\boldsymbol{T}\cdot\boldsymbol{R})^2 + (\boldsymbol{S}\cdot\boldsymbol{R})^2]^{\frac{1}{2}}. \tag{39}$$

The two solutions χ_1 and χ_2 differ by $\frac{1}{2}\pi$, thus ensuring orthogonality of $|\psi_1\rangle$ and $|\psi_2\rangle$.

Now let $\boldsymbol{R}$ vary round a circuit C surrounding the origin (figure 8). Then (and only then) the complex number $\boldsymbol{T}\cdot\boldsymbol{R} + \mathrm{i}\boldsymbol{S}\cdot\boldsymbol{R}$ makes a circuit that encloses the origin of the complex plane. Thus χ_1 and χ_2 each change by π round C, so that $|\psi_1\rangle$ and $|\psi_2\rangle$

change sign. The importance of this sign change as a test for diabolical points was emphasized by Longuet-Higgins (1975) (see also Uhlenbeck 1976; Mead 1979, 1980, 1983; Mead & Truhlar 1979). Berry (1984) has generalized the theory to Hermitian (rather than real symmetric) Hamiltonians, and calculated the phase factor that replaces the sign change.

We apply the circuit test to the normal derivative $u(s)$ of the wavefunction at the point s on the boundary of the triangle. From (38),

$$u(s) = u_1^*(s)\cos\chi + u_2^*(s)\sin\chi, \tag{40}$$

where $u_1^*(s)$ and $u_2^*(s)$ are the normal derivatives of the degenerating waves at the same boundary point. Defining

$$u_1^*(s) \equiv u^*(s)\cos Z(s), \quad u_2^*(s) \equiv u^*(s)\sin Z(s), \tag{41}$$

we can write the circuit test function (40) (in a more explicit notation) as

$$u(s;\boldsymbol{R}) = u^*(s)\cos\{\chi(\boldsymbol{R}) - Z(s)\}. \tag{42}$$

The circuit was chosen as a circle in the X–Y plane, parametrized by its angle θ (figure 8) reckoned from the X-axis. A lengthy but elementary calculation based on (39) shows that the variation of u with θ, for any s, is given by a member of a two-parameter family of universal functions. The result is

$$u = u^*(s)\left\{\frac{1}{2}\left[1 - \frac{\sin(\theta'+\beta')}{[\sin^2(\theta'+\beta') + V'^2\sin^2\theta']^{\frac{1}{2}}}\right]\right\}^{\frac{1}{2}}, \tag{43}$$

where

$$\left.\begin{aligned} \theta' &\equiv \theta - \tfrac{1}{2}\pi + \arctan\left[\frac{V\cot 2Z\sin\sigma - \sin\tau}{V\cot 2Z\cos\sigma - \cos\tau}\right], \\ V'^2 &\equiv \left[\frac{1+V^2+(V^2-1)\cos 4Z - 2V\cos\beta\sin 4Z}{1+V^2-(V^2-1)\cos 4Z + 2V\cos\beta\sin 4Z}\right]^{\frac{1}{2}}, \\ \tan\beta' &\equiv \frac{2V\sin\beta}{(V^2-1)\sin 4Z + 2V\cos\beta\cos 4Z}, \quad 0 \leqslant \beta' \leqslant \pi. \end{aligned}\right\} \tag{44}$$

The circuit test function changes sign exactly once round C and the shifted angle θ' is defined so that the zeros of u lie at $\theta' = 0$ and $\theta' = 2\pi$.

The prediction of this theory is that the normal derivative at any point s will vary round C according to the function (43) for some choice of β' and V', provided C is small enough for the local analysis to apply. The two states $|\psi_1\rangle$ and $|\psi_2\rangle$ correspond to the two signs of the inner square root in (43), and this shows that their boundary normal derivatives vary round C in exactly the same way, apart from a relative shift of π in θ or θ'.

For all diabolical points in table 1, the circuit test gave the predicted sign change. Figures 9*a* and *b* show how u_1 and u_2 vary round a small circle (radius 0.1) in the X–Y plane, for the two lowest diabolical points (levels 5 and 6, and levels 6 and 7).

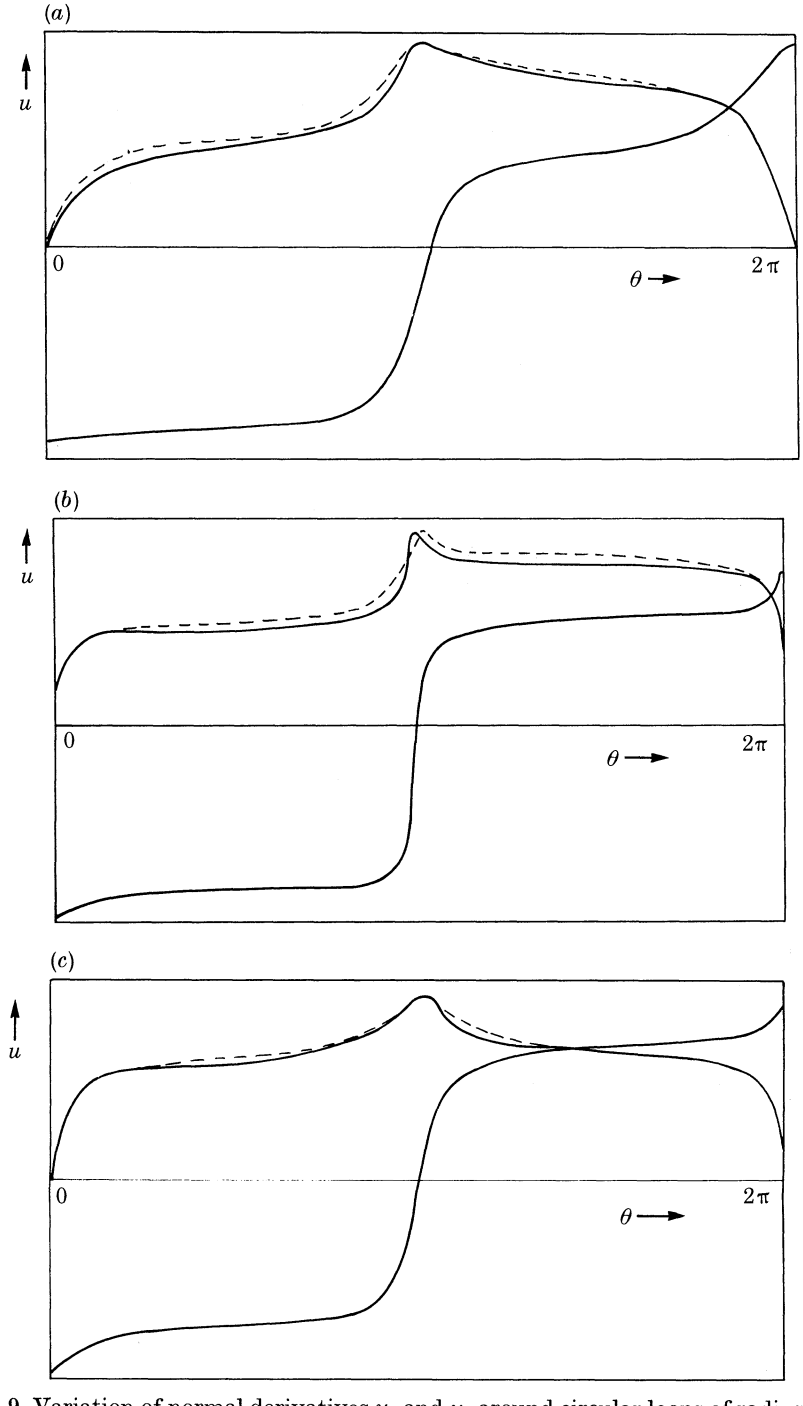

FIGURE 9. Variation of normal derivatives u_1 and u_2 around circular loops of radius 0.1 in the X–Y plane, centred on degeneracies. The dashed curves are fits by the theoretical formula (43). (*a*) Diabolical point involving levels 5 and 6 (fitted by $\beta' = 30°$ and $V' = 2$). (*b*) Diabolical point involving levels 6 and 7 (fitted by $\beta' = 12°$, $V' = 2$. (*c*) Symmetry degeneracy involving levels 3 and 4 (fitted by $\beta' = 45°$, $V' = 5$).

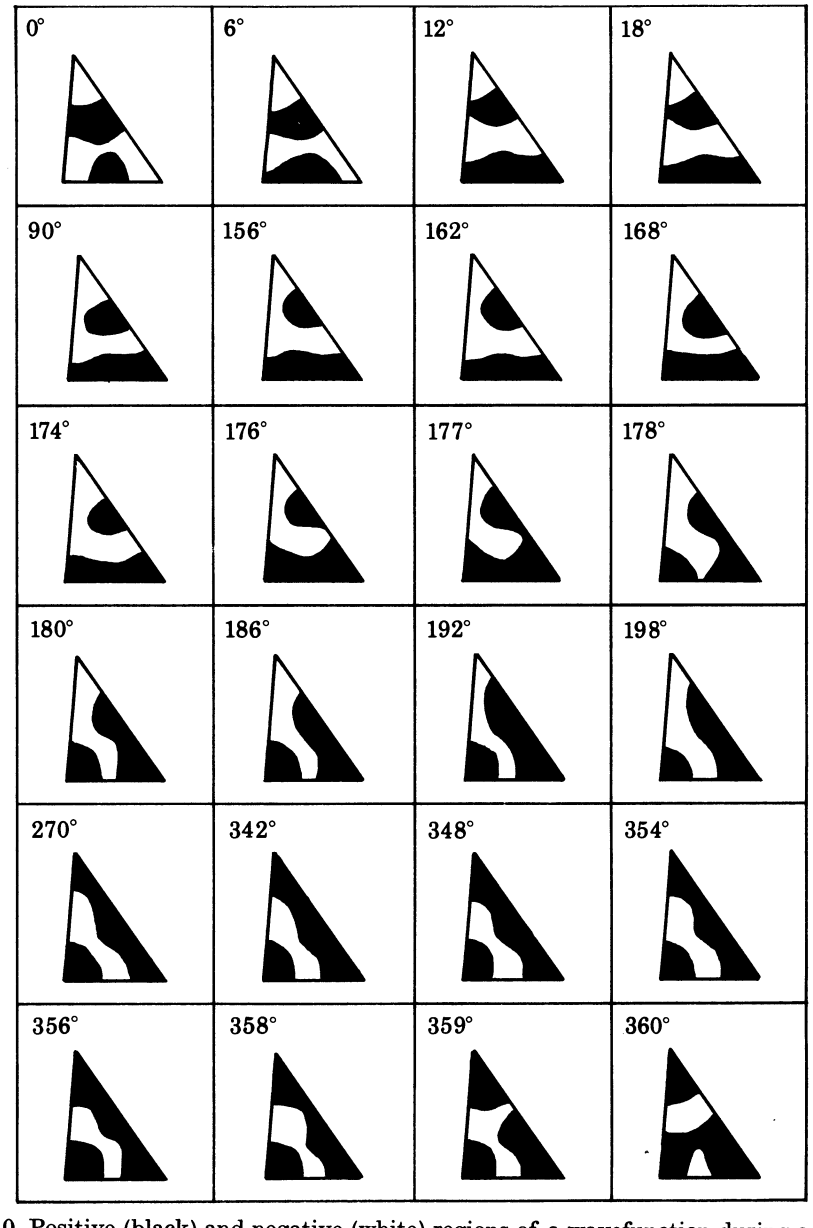

FIGURE 10. Positive (black) and negative (white) regions of a wavefunction during a circuit (in the X–Y plane) of the diabolical point between levels 6 and 7, for the angles indicated (measured from the X axis).

The values of u were calculated for a point $s = \frac{1}{5}\mathscr{L}$, measured from the corner α in the direction of β. To a close approximation the curves of u_1 and u_2 are the same apart from a shift of π, and are well fitted by (43) with a suitable choice of V' and β'. Figure 9*c* shows similar behaviour of u_1 and u_2 for the symmetry degeneracy between levels 3 and 4.

In figure 9 the circuit angle θ is measured from the X-direction and yet the curves are well fitted, without θ shifting, by (43), which involves θ'. The explanation is that the cones are elongated in the X-direction, so that the larger of the two vectors $\boldsymbol{S}$ and $\boldsymbol{T}$ is directed near the Y-direction; the near-equality of θ and θ' (up to π) now follows from (44) provided V is not close to unity (i.e. when the cones are elongated). It is possible that the X-elongation is an artefact of the choice of parameters X, Y describing triangles.

The sign changes of $|\psi_1\rangle$ and $|\psi_2\rangle$ round C imply that the pattern of nodal lines of the wavefunctions $\psi_1(\boldsymbol{r})$ and $\psi_2(\boldsymbol{r})$ must change round C, in order to produce the reversal of positive and negative regions. Generically, that is for an arbitrary point on C, nodal lines do not cross (Berry 1983*b*), but they may stably do so in a one-parameter deformation such as C (Uhlenbeck 1976). If at any point on C the positive and negative regions of ψ are equal in number and all nodal lines hit the boundary, then such nodal crossings need not occur, and the sign reversal can be accomplished by the whole nodal pattern sliding round within the triangle. This occurs for example around the symmetry degeneracy between levels 2 and 3.

But crossings may occur even when they need not. Figure 10 shows the nodal rearrangements round the diabolical point involving levels 6 and 7. There are five 'redundant' nodal crossings; four occur on the boundary (near $\theta = 18°$, between 176° and 177°, between 171° and 178°, and between 358° and 359°), and one within the triangle (between 359° and 360°). Note the extremely rapid pattern changes near $\theta = 0° = 360°$ and $\theta = 180°$, which are a consequence of the elongation of the cones. Despite the complex sequence of changes, at each point $\boldsymbol{r}$, ψ reverses sign only once during the circuit.

Korsch (1983) gives a very clear picture of nodal rearrangements around a symmetry degeneracy of the square billiard, as well as illustrating the nodal patterns in a parallelogram as its angles vary.

6. Asymptotic theory for thin triangles

The computational technique based on the determinant Δ (13)–(15) converges slowly for thin triangles (γ and Y small); and it is then desirable to check the computations against an analytical theory, to be sure that no degeneracies have been missed.

The theory is based on the observation that exact solutions of the wave equation, vanishing on sides issuing from a corner with angle γ, are

$$\psi_l(r, \phi) = J_{\pi l/\gamma}(kr) \sin(\pi l \phi/\gamma), \quad l = 1, 2, 3, \ldots, \tag{45}$$

where r and ϕ are polar coordinates with the corner as origin (figure 11), and J denotes a Bessel function (Abramowitz & Stegun 1964). The solution which also vanishes on the third side is in general a superposition of these Bessel waves with different l.

When γ is small, however, waves with $l > 1$ contribute very little to the low-lying states. There follows from this a theory which we will work out, and compare with computation, for the two kinds of isosceles thin triangle ($\gamma \ll \pi$, $\alpha = \beta \approx \frac{1}{2}\pi$, i.e. Y small and $X = 9$; and $\gamma = \beta \ll \pi$, $\alpha \approx \pi$, i.e. Y small and $X = 0$). Generalization to thin non-isosceles triangles is possible but cumbersome.

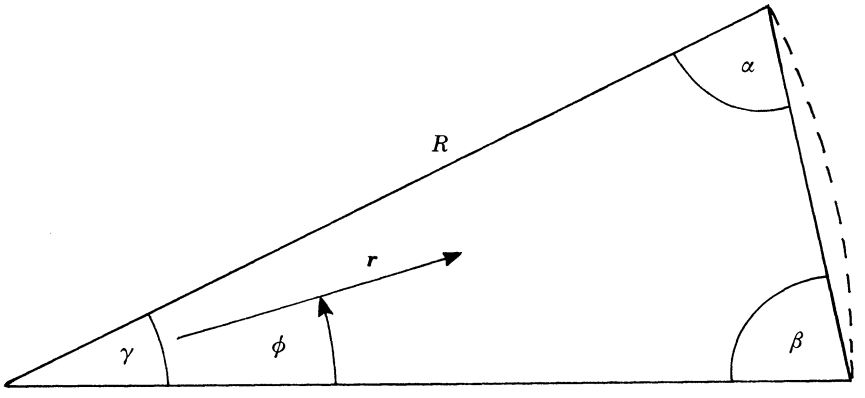

FIGURE 11. Coordinates for theory of thin triangle with $\alpha = \beta$.

Consider first the case $\alpha = \beta$ (figure 11). The Bessel functions of order π/γ which vanish on the circle $r = R$, where R is the length of the long sides of the triangle, will be good approximations to eigenfunctions of the triangle, because for small γ the short side nearly coincides with part of the circle. The condition for an eigenvalue k_j can therefore be written as

$$J_{\pi/\gamma}(k_j R) = 0, \tag{46}$$

and k_j and R can be eliminated in favour of E_j and γ by using (2) and the relation between R, γ and the area $\mathscr{A}$, which gives

$$k_j R = 2(2\pi E_j/\gamma)^{\frac{1}{2}}. \tag{47}$$

Bessel functions of large order (small γ) can be approximated uniformly in their arguments by means of Airy functions, and standard formulae (Abramowitz & Stegun 1964) enable (46) to be replaced by

$$\mathrm{Ai}\,(-(\pi/\gamma)^{\frac{2}{3}}\zeta) = 0, \tag{48}$$

where

$$\zeta \equiv \{\tfrac{3}{2}[(Z^2-1)^{\frac{1}{2}} - \arccos(1/Z)]\}^{\frac{2}{3}}, \tag{49}$$

and

$$E = \pi Z^2/8\gamma. \tag{50}$$

If a_j is the (tabulated) jth zero of the Airy function, (48) gives

$$\zeta = a_j/(\pi/\gamma)^{\frac{2}{3}}, \tag{51}$$

from which (49) gives Z implicitly and thence E_j from (50).

All the states thus obtained have even parity with respect to the symmetry line bisecting γ. The first states with odd parity involve Bessel functions of order $2\pi/\gamma$

(cf. 45) and it is not hard to show that if $0 \leqslant Y \leqslant 0.6$ (the range not covered by figure 7*a*) no such states have energies $0 < E_j < 18$ which was the range of our computations.

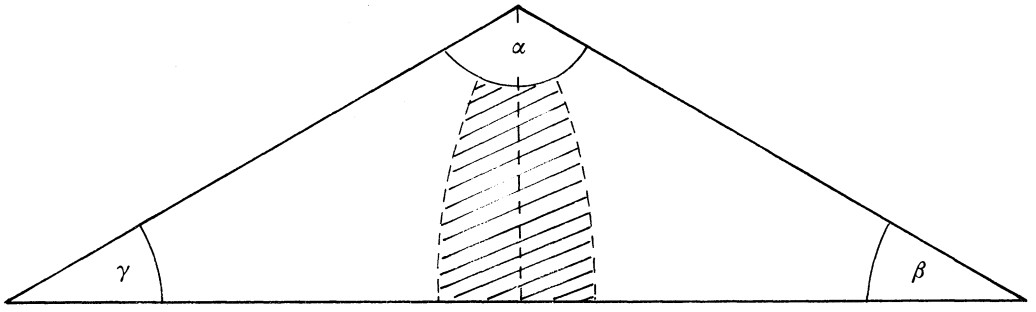

FIGURE 12. Thin triangle with $\gamma = \beta$. States have even or odd parity about the symmetry line.

TABLE 2. LOW-LYING LEVELS OF THIN ISOSCELES TRIANGLES

$\gamma = 6°, \alpha = \beta = 87°$ ($X = 9$, $Y = 0.6$)

level number j	E_j (analytic theory)	E_j (computed by determinant)
1	5.429	5.44
2	7.036	7.05
3	8.608	8.62
4	10.212	10.21
5	11.870	11.87

$\gamma = \beta = 10°, \alpha = 160°$ ($X = 0$, $Y = 1$)

level number j	E_j (analytic theory)	E_j (computed by determinant)
1	5.664	5.69
2	7.512	7.58
3	9.040	9.05
4	10.655	10.74

Now consider the case $\beta = \gamma$ (figure 12). States have odd or even parity about the symmetry line and can be found by matching states of the type (45) based on the β and γ corners. The match is imperfect in the shaded region of figure 12 but this gets thinner as the triangle does. For odd states, the Bessel functions vanish on the radius corresponding to the symmetry line, and the states are formed simply by adjoining two copies of the states of the $\alpha = \beta$ isosceles triangle. For even states, the Bessel functions must have zero slope at the symmetry radius. The result is that the levels of these $\beta = \gamma$ triangles are given by (49)–(51) with the factor 8 replaced by 4 in (50) and with the zeros a'_j of the derivatives of the Airy function included in (51) as well as a_j.

Table 2 gives the lowest levels computed by this theory for the 6°, 87°, 87° isosceles triangle ($Y = 0.6$ and $X = 9$, corresponding to the left-hand edge of

figure 7*a*), and for the 10°, 10°, 160° isosceles triangle ($Y = 1$ and $X = 0$), together with levels computed by the determinantal method of § 3. The agreement is very good. It becomes much less good if the uniformity of the approximation embodied in (49)–(51) is degraded by approximating the function $\zeta(Z)$ for Z close to unity, or the zeros a_j or a'_j by their large-j asymptotic forms.

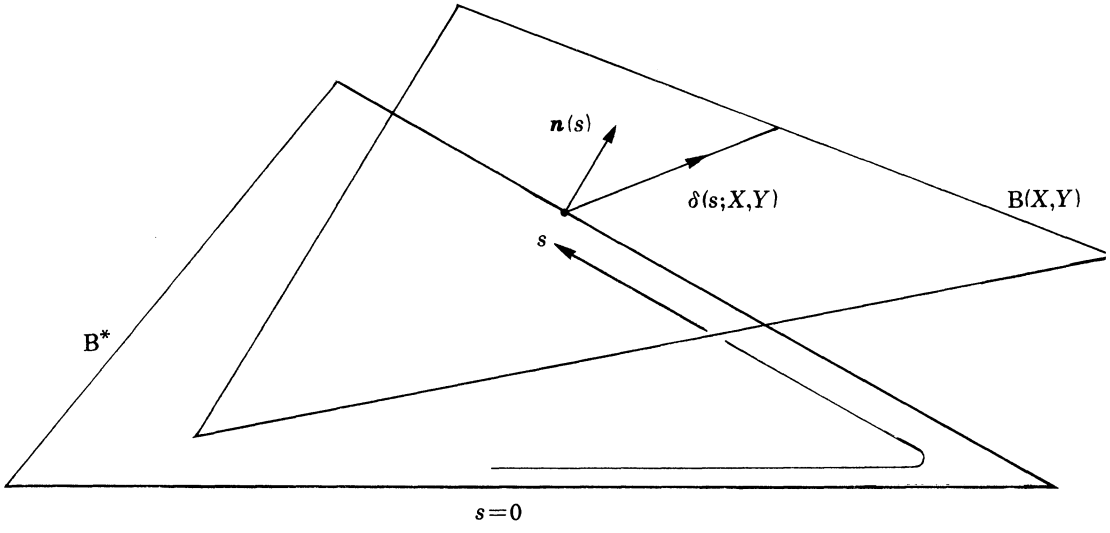

FIGURE 13. Boundary displacement $\boldsymbol{\delta}(s; X, Y)$ taking diabolical triangle B* to deformed triangle B(X, Y).

7. ESTIMATE OF DENSITY OF DIABOLICAL POINTS

We shall obtain a scaling law for the increase with j of the number of degeneracies between energy level surfaces $E_j(X, Y)$ and $E_{j+1}(X, Y)$ in a given region of triangle space X, Y. The average spacing of the surfaces, $S(= E_{j+1} - E_j)$, is unity (cf. (27)–(29)) and they are conically connected. For small S, each cone has a 'domain' whose area $\mathscr{A}_d(S)$ can be estimated in terms of the linear theory of § 5, provided the rate of increase of the energy separation (ΔE on figure 8) with X and Y is known. From (32)–(34), this rate of increase is proportional to the derivatives with respect to deformations of the matrix elements H'_{ij}, defined by (31).

It is shown in appendix A that if the triangle boundary B(X, Y) is obtained from the diabolical boundary B* by displacing the point s on the boundary of B* by $\boldsymbol{\delta}(s; X, Y)$ (figure 13), the matrix elements are

$$H'_{ij}(X, Y) = \frac{-\mathscr{A}}{4\pi} \oint \mathrm{d}s\, \boldsymbol{n}(s) \cdot \boldsymbol{\delta}(s; X, Y)\, u_i^*(s)\, u_j^*(s), \quad i, j = 1, 2, \tag{52}$$

where u_i^* denotes the normal boundary derivatives of the degenerating states $|\psi_1^*\rangle$ and $|\psi_2^*\rangle$. Also proved in appendix A are the vanishing of H'_{ij} under displacements $\boldsymbol{\delta}(s)$ corresponding to rigid motions of B*, and the trivial scaling of H'_{ij} under homogeneous dilation of B*. Under the non-trivial deformations represented by X and

Y, the components of $\boldsymbol{\delta}$ vary linearly. We are concerned with the dependence on E, that is on level number j or wavenumber k, and this is embodied in u_i^* as we now describe.

The u_i^* are gradients of $\psi_i^*(\boldsymbol{r})$ which oscillate with wavelength roughly $2\pi/k$, and so the u_i^* scale as k (an explicit example is the normalization law (A 23)). According to (32) and (52), the energy spacing S depends on integrals of $(u_1^{*2}-u_2^{*2})$ and $u_1^*u_2^*$, whose values fluctuate positively and negatively round B*. Orthogonality of u_1^* and u_2^* imparts a degree of incoherence and gives rise to destructive interference whose effect can be estimated by modelling $u_1^*(s)$ and $u_2^*(s)$ by independent sets of k random numbers (one sample of $u_1^*(s)$ per wavelength round B^*). This reduces the values of $(u_1^2-u_2^2)$ and u_1u_2 by a factor $k^{\frac{1}{2}}$: a result confirmed by a more careful calculation in which $u_1^*(s)$ and $u_2^*(s)$ are modelled by independent gaussian random functions with a suitably-chosen autocorrelation function. Thus the H'_{ij} and also their X and Y derivatives, are estimated to scale as $k\times k\times k^{-\frac{1}{2}}$, i.e. as $k^{\frac{3}{2}}\sim E^{\frac{3}{4}}\sim j^{\frac{3}{4}}$: the cones get thinner as j increases.

For small spacings S the principal cone radii $R_\pm$ scale as $Sk^{-\frac{3}{2}}$, and the area $\mathscr{A}_{\rm d}(S)=\pi R_+R_-$ scales as $S^2k^{-3}\sim S^2j^{-\frac{3}{2}}$. We seek the density $\rho_{\rm d}(j)$ of degeneracies between levels j and $j+1$ in the X–Y plane. This is connected via $\mathscr{A}_{\rm d}(S)$ to the *level spacing distribution* $P(S)$ (probability density for spacing S) by

fraction of area of X–Y plane for which spacing is less than S equals

$$\int_0^S \mathrm{d}S'P(S')=\rho_{\rm d}(j)\,\mathscr{A}_{\rm d}(S)\sim\rho_{\rm d}(j)\,k^{-3}S^2, \tag{53}$$

so that

$$P(S)\sim\rho_{\rm d}(j)\,k^{-3}S,\quad\text{as}\quad S\to 0. \tag{54}$$

The 'linear level repulsion' for small S is expected for any system with diabolical points (Berry 1981, 1983*b*). Moreover, the slope of $P(S)$ at the origin should be of order unity for generic systems (Porter 1965). In the present case this is confirmed by figure 14 which shows $P(S)$ computed from about 400 spacings. The histogram is well fitted within the accuracy of the data by the Wigner distribution

$$P(S)=\tfrac{1}{2}\pi S\exp\{-\tfrac{1}{4}\pi S^2\}, \tag{55}$$

shown as a dashed line in figure 14 (the 'exact' slope should be $\frac{1}{6}\pi^2$ (Porter 1965) but this is immaterial in the present context).

Equations (54) and (55) together imply that the degeneracy density $\rho_{\rm d}(j)\sim k^3\sim j^{\frac{3}{2}}$. For the *total number* $\mathscr{N}_{\rm d}(j)$ of degeneracies in the whole X–Y rectangle up to and including those between levels j and $j+1$ (labelled $j+\frac{1}{2}$), this gives the estimate

$$\mathscr{N}_{\rm d}(j)=\sum_{j'=1}^{j}\rho(j')\propto(j+\tfrac{1}{2})^{\frac{5}{2}}. \tag{56}$$

This asymptotic estimate should become more accurate as j increases. Nevertheless, we shall test it using the limited data of table 1. Including all degeneracies, symmetry-related as well as diabolical because they too have conical neighbourhoods,

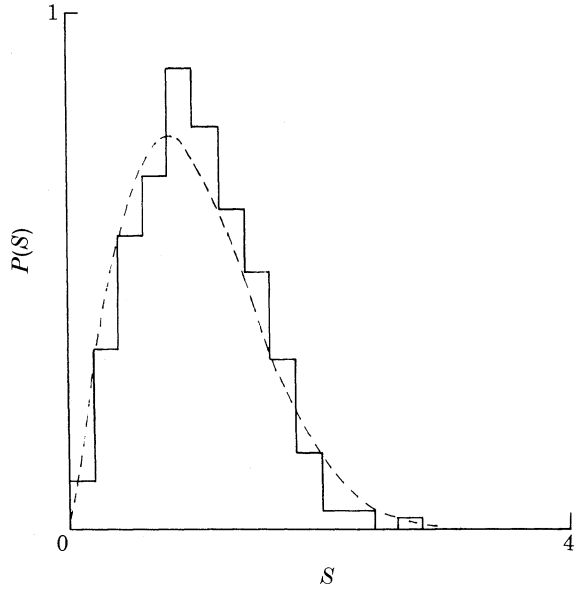

FIGURE 14. Probability distribution $P(S)$ of the level spacings S in the range $1 \leqslant X \leqslant 8$, $1.6 \leqslant Y \leqslant 4$, $E > 12$. The dashed line is the Wigner distribution (55).

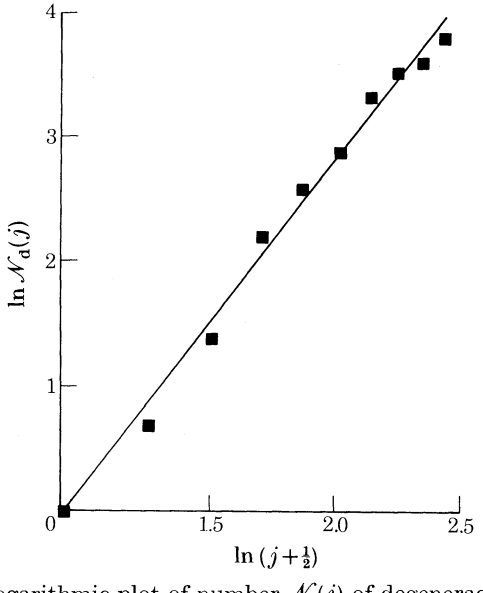

FIGURE 15. Double logarithmic plot of number $\mathcal{N}(j)$ of degeneracies below and including those between levels j and $j+1$. The straight line has slope 2.5 (cf. (56)).

we obtain the double logarithmic graph of figure 15. The points are well fitted by the straight line which is drawn with the 'theoretical' slope $\frac{5}{2}$. We have confirmed that the fit is not significantly affected by (approximately) including the 'perimeter' and 'corner' corrections embodied in (27)–(29).

Concluding remarks

Using the family of all triangles as an illustrative example, we have studied degeneracies occurring in the spectra of families of generic real Hermitian operators. By applying the sign-reversal test we have confirmed that the energy eigenvalue surfaces are conically connected, so that the degeneracies are diabolical points. Some of the degeneracies are expected, and found, for symmetric triangles. This naturally raises the question of whether the diabolical triangles of table 1 might possess some hidden symmetry. We think the answer is negative but cannot give a proof. From any degeneracy it appears possible to construct an operator that commutes with $\hat{H}$ (Valkering & Caspers 1973), but this does not appear to be associated with any geometric symmetry of H^*, and as pointed out in § 4 the angles of diabolical triangles are not close to rational multiples of π.

The conical degeneracies are expected to occur for two-parameter families of generic real Hamiltonians. Special classes of Hamiltonian may have different degeneracies. For example, energy levels of Hamiltonians which are *separable* can degenerate when only a single parameter is varied, so that for two parameters X, Y the energy surfaces intersect in lines. One case in which this occurs is when X and Y are parameters in a two-dimensional potential with circular symmetry: the crossing levels correspond to different angular momenta. Another special class is one-dimensional Hamiltonians with fixed-end or vanishing-at-infinity boundary conditions, for which degeneracies are strictly forbidden, so that even an infinite of parameters X, Y, ..., will not produce them.

A quite different way to embed a given Hamiltonian in a two-parameter family is to consider it as a member of a family labelled by a single *complex* parameter C. It is possible for levels to degenerate at isolated points in the C-plane (even for one-dimensional problems; see Bender & Orszag 1978). But for complex C the operators are not Hermitian, the eigenvalues are not real, and at degeneracies their 'surfaces' have a branch-point, rather than conical, structure.

On the other hand, if the operators are Hermitian but not real (e.g. if magnetic fields are present), *three* real parameters must typically be varied to produce a degeneracy (Von Neumann & Wigner 1929).

Finally we remark that degeneracies involving more than two levels can be made to occur by varying more parameters. These higher degeneracies have been systematically studied by Caspers (1968) and Arnold (1978). The simplest case is degeneracies of three levels, and typically requires five parameters (for real Hamiltonians), so that numerical exploration of higher degeneracies is daunting.

M. V. B. thanks Professor Th. W. Ruijgrok for extensive discussions and for carrying out stimulating exploratory computations, and the Institute of Theoretical Physics, University of Utrecht for its generous hospitality during the initial phases of this work. M. W. was supported by an S.E.R.C. postgraduate award.

References

Abramowitz, M. & Stegun, I. A. (eds) 1964 *Handbook of mathematical functions*. Washington: U.S. National Bureau of Standards.

Arnold, V. I. 1978 *Mathematical methods of classical mechanics*. New York: Springer.

Balian, R. & Bloch, C. 1972 *Ann. Phys.* **69**, 76–160.

Baltes, H. P. & Hilf, E. R. 1976 *Spectra of finite systems*. Mannheim: B. I. Wissenschaftsverlag.

Bender, C. M. & Orszag, S. A. 1978 *Advanced mathematical methods for scientists and engineers*. New York: McGraw-Hill.

Berry, M. V. 1981 *Ann. Phys.* **131**, 163–216.

Berry, M. V. 1983*a* In *Proceedings of the* 1982 *De Broglie Symposium on Wave-particle Dualism, Perugia, Italy* (ed. S. Diner & D. Fargue). Dordrecht: D. Reidel.

Berry, M. V. 1983*b* Semiclassical mechanics of regular and irregular motion. In *Chaotic behavior of deterministic systems*, Les Houches Lectures XXXVI (ed. G. Iooss, R. H. G. Helleman & R. Stora), pp. 171–271. Amsterdam: North-Holland.

Berry, M. V. 1984 *Proc. R. Soc. Lond.* A. **392**, 45–57.

Berry, M. V. & Hannay, J. H. 1977 *J. Phys.* A **10**, 1809–1821.

Berry, M. V. & Tabor, M. 1977 *Proc. R. Soc. Lond.* A **356**, 375–394.

Berry, M. V. & Upstill, C. 1980 *Prog. Optics* **XVIII**, 257–346.

Bunimovich, L. A. 1974 *Funct. Anal. Appl.* **8**, 254–255.

Caspers, W. J. 1968 *Physica* **40**, 125–138.

Dehareng, D., Chapuisat, X., Lorquet, J-C., Galloy, C. & Raseev, G. 1983 *J. chem. Phys.* **78**, 1246–1264.

De Mey, G. 1976 *Int. J. Numer. Meth. Engng* **10**, 59-66.

Desouter-Lecomte, M., Galloy, C. & Lorquet, J-C. 1979 *J. chem. Phys.* **71**, 3661–3672.

Gutkin, E. 1983 *Dynamical Systems* (Submitted.)

Herzberg, G. & Longuet-Higgins, H. C. 1963 *Discuss. Faraday Soc.* **35**, 77–82.

Hill, D. L. & Wheeler, J. A. 1952 *Phys. Rev.* **89**, 1102–1145.

Jung, C. G. 1980 *Can. J. Phys.* **58**, 719–728.

Knox, R. S. & Gold, A. 1964 *Symmetry in the solid state*. New York: Benjamin.

Korsch, H. J. 1983 *Physics Lett.* **97**A, 77–80.

Longuet-Higgins, H. C. 1975 *Proc. R. Soc. Lond.* A **344**, 147–156.

Marcus, R. A. 1980 In *Nonlinear dynamics* (ed. R. H. G. Helleman), pp. 169–182. *Ann. N.Y. Acad. Sci.* **357**.

Mead, C. A. 1979 *J. chem. phys.* **70**, 2276–2283.

Mead, C. A. 1980 *Chem. Phys.* **49**, 23–32; 33–38.

Mead, C. A. 1983 *J. chem. Phys.* **78**, 807–814.

Mead, C. A. & Truhlar, D. G. 1979 *J. chem. Phys.* **70**, 2284–2296.

Niwa, Y., Kobayashi, S. & Kitahara, M. 1980 In *Developments in boundary element methods* 2 (ed. P. K. Banerjee & R. Shaw), pp. 143–176. London: Appl. Sci. Publications.

Noid, D. W., Koszykowski, M. L., Tabor, M. & Marcus, R. A. 1980 *J. chem. Phys.* **72**, 6167–6175.

Pinsky, M. 1980 *SIAM Jl math. Anal.* **11**, 819–827.

Porter, C. E. (ed.) 1965 *Statistical theory of spectra: fluctuations*. New York: Academic Press.

Richens, P. J. & Berry, M. V. 1981 *Physica* **1D**, 495–512.

Riddell, R. J. Jr 1979 *J. Comput. Phys.* **31**, 21–41; 42–59.

Sinai, Ya. G. 1970 *Russ. math. Surv.* **25**, 137–189.

Sinai, Ya. G. 1976 *Introduction to ergodic theory*. Princeton University Press.

Tai, G. R. C. & Shaw, R. P. 1974 *J. acoust. Soc. Am.* **56**, 796–804.

Teller, E. 1937 *J. phys. Chem.* **41**, 109–116.

Uhlenbeck, K. 1976 *Am. J. Math.* **98**, 1059–1078.

Valkering, T. P. & Caspers, W. J. 1973 *Physica* **63**, 113–138.

Vaz Pires, M., Galloy, C. & Lorquet, J-C. 1978 *J. chem. Phys.* **69**, 3242–3249.

Von Neumann, J. & Wigner, E. 1929 *Phyz. Z.* **30**, 467–470.

Zemlyakov, A. N. & Katok, A. B. 1975 *Math. Z.* **18**, 291–294. (English translation *Math. Notes* **18** (1976), 760–764.)

Appendix A. Matrix elements for triangle deformations

First, we derive the formula (52) for the Hamiltonian matrix elements H'_{ij}. Let the Hermitian operator corresponding to equation (1) with energy k^2 be $\hat{\mathscr{H}}$. Then matrix elements of the operator $\hat{H}$ associated with energy E are given (cf. (2)) by

$$H_{ij} = (\mathscr{A}/4\pi)\mathscr{H}_{ij}. \tag{A 1}$$

To find the deformation matrix elements $\mathscr{H}'_{ij}$ corresponding to (31), it is convenient to first soften the boundaries and represent the unperturbed (diabolical) triangle B* by a potential $V(\boldsymbol{r})$ which is small within B* and rises rapidly beyond the boundary of B*. Thus

$$\hat{\mathscr{H}} = -\nabla^2 + V(\boldsymbol{r}). \tag{A 2}$$

To obtain the deformed boundary, deform the contours of V at each point $\boldsymbol{r}$ by $\boldsymbol{\delta}(\boldsymbol{r})$, so that

$$V(\boldsymbol{r}) \to V(\boldsymbol{r} - \boldsymbol{\delta}(\boldsymbol{r})). \tag{A 3}$$

Thus the deformation matrix element for states $|\psi_i\rangle$ and $|\psi_j\rangle$ becomes, to first order in $\boldsymbol{\delta}$,

$$\begin{aligned}\mathscr{H}'_{ij} &= \langle\psi_i|\, V(\boldsymbol{r} - \boldsymbol{\delta}(\boldsymbol{r})) - V(\boldsymbol{r})\,|\psi_j\rangle \\ &= -\int\int_{\mathscr{A}} \mathrm{d}\boldsymbol{r}\psi_i(\boldsymbol{r})\,\psi_j(\boldsymbol{r})\,\boldsymbol{\delta}(\boldsymbol{r})\cdot\nabla V(\boldsymbol{r}).\end{aligned} \tag{A 4}$$

Now we must take the limit as $V(r)$ hardens into a sharp high wall and $\psi_i(r)$ vanishes outside B*. Then the integration in (A 4) is confined to a thin boundary ribbon. Using coordinates s (round the boundary) and z (perpendicular to the boundary and increasing outwards), we obtain

$$\mathscr{H}'_{ij} = -\oint \mathrm{d}s\,\boldsymbol{n}(s)\cdot\boldsymbol{\delta}(s)\,I(s), \tag{A 5}$$

where

$$I(s) \equiv \int_{-\infty}^{\infty} \mathrm{d}z\,\psi_i\,\psi_j\,\frac{\partial V}{\partial z}(z, s) \tag{A 6}$$

and $\boldsymbol{\delta}(s)$ denotes $\boldsymbol{\delta}(\boldsymbol{r}(s))$. Integration by parts gives

$$I(s) = -\int_{-\infty}^{\infty} \mathrm{d}z\left(V\psi_i\frac{\partial\psi_j}{\partial z} + V\psi_j\frac{\partial\psi_i}{\partial z}\right). \tag{A 7}$$

The next step is to eliminate V by using the wave equation

$$V\psi_i = (\nabla^2 + k_i^2)\,\psi_i. \tag{A 8}$$

It is convenient to write ψ_i as

$$\psi_i = \psi_i^{\mathrm{int}} f(z), \tag{A 9}$$

where ψ_i^{int} is an interior wavefunction satisfying (1), and $f(z)$ is a cutoff function falling smoothly from 1 to 0 as z increases through zero. Equation (A 8) now becomes

$$V\psi_i = 2(\partial\psi_i^{\mathrm{int}}/\partial z)f' + \psi_i^{\mathrm{int}} f'', \tag{A 10}$$

where the prime denotes differentiation with respect to z. Near the boundary,

$$\psi_i^{\text{int}} = u_i(s)\, z, \tag{A 11}$$

where u_i is the normal derivative of $|\psi_i\rangle$. Equation (A 7) now becomes

$$I(s) = -2u_i(s)\, u_j(s) \int_{-\infty}^{\infty} \mathrm{d}z (2f' + zf'')(f + zf'). \tag{A 12}$$

Expansion and repeated integration by parts leads to

$$\begin{aligned} I(s) &= -u_i(s)\, u_j(s) \int_{-\infty}^{\infty} \mathrm{d}z (f^2)' \\ &= +u_i(s)\, u_j(s), \end{aligned} \tag{A 13}$$

thus

$$\mathscr{H}'_{ij} = -\oint \mathrm{d}s\, \boldsymbol{n}(s) \cdot \boldsymbol{\delta}(s)\, u_i(s)\, u_j(s) \tag{A 14}$$

and (52) follows directly on using (A 1). (This result can alternatively be derived by minimizing the field Lagrangian for the wave equation.)

Secondly, we prove that $\mathscr{H}'_{ij}$ vanishes when $\boldsymbol{\delta}(s)$ represents rigid translations and rotations, and scales correctly for homogeneous dilations. To do this we rewrite (A 14) as integrals over the triangle area $\mathscr{A}$ in three different ways, whose equivalence rests on the fact that $\nabla\psi_i$ is parallel to $\boldsymbol{n}$ on the boundary:

$$\mathscr{H}'_{ij} = -\oint \mathrm{d}s\, \boldsymbol{n} \cdot \boldsymbol{\delta} (\nabla\psi_i \cdot \nabla\psi_j) = -\iint_{\mathscr{A}} \mathrm{d}\boldsymbol{r}\, \nabla \cdot (\boldsymbol{\delta} \nabla\psi_i \cdot \nabla\psi_j), \tag{A 15a}$$

$$= -\oint \mathrm{d}s\, \boldsymbol{n} \cdot \nabla\psi_i \boldsymbol{\delta} \cdot \nabla\psi_j = -\iint_{\mathscr{A}} \mathrm{d}\boldsymbol{r}\, \nabla \cdot (\nabla\psi_i \boldsymbol{\delta} \cdot \nabla\psi_j), \tag{A 15b}$$

$$= -\oint \mathrm{d}s\, \boldsymbol{n} \cdot \nabla\psi_j \boldsymbol{\delta} \cdot \nabla\psi_i = -\iint_{\mathscr{A}} \mathrm{d}\boldsymbol{r}\, \nabla \cdot (\nabla\psi_j \boldsymbol{\delta} \cdot \nabla\psi_i). \tag{A 15c}$$

Next we write $\mathscr{H}'_{ij}$ as $(b) + (c) - (a)$. Repeated use of vector identities, together with the perpendicularity of $\nabla \times \boldsymbol{\delta}$ to the $\boldsymbol{r}$ plane and the wave equation (1) for ψ_i with $k_1 = k_2 = k$, gives

$$\begin{aligned} \mathscr{H}'_{ij} = \iint_{\mathscr{A}} \mathrm{d}\boldsymbol{r} [k^2 \boldsymbol{\delta} \cdot \nabla(\psi_i \psi_j) + \nabla\psi_i \cdot \nabla\psi_j \nabla \cdot \boldsymbol{\delta} \\ - \{\nabla\psi_i \cdot (\nabla\psi_j \cdot \nabla) + \nabla\psi_j \cdot (\nabla\psi_i \cdot \nabla)\} \boldsymbol{\delta}]. \end{aligned} \tag{A. 16}$$

Now

$$\boldsymbol{\delta} \cdot \nabla(\psi_i \psi_j) = \nabla \cdot (\boldsymbol{\delta} \psi_i \psi_j) - \psi_i \psi_j \nabla \cdot \boldsymbol{\delta}. \tag{A 17}$$

The divergence integrates to a boundary term that vanishes as a result of ψ_i vanishing, and

$$\begin{aligned} \mathscr{H}'_{ij} = -\iint_{\mathscr{A}} \mathrm{d}r [(k^2 \psi_i \psi_j - \nabla\psi_i \cdot \nabla\psi_j) \nabla \cdot \boldsymbol{\delta} \\ + \{\nabla\psi_i \cdot (\nabla\psi_j \cdot \nabla) + \nabla\psi_j \cdot (\nabla\psi_i \cdot \nabla)\} \boldsymbol{\delta}] \end{aligned} \tag{A 18}$$

is left.

We consider the following three deformations:

$$\left.\begin{aligned} &\text{translation:} && \boldsymbol{\delta}(\boldsymbol{r}) = \text{constant};\\ &\text{rotation:} && \boldsymbol{\delta}(\boldsymbol{r}) = \boldsymbol{\Omega}\times\boldsymbol{r}\ (\boldsymbol{\Omega}\text{ perpendicular to the }\boldsymbol{r}\text{ plane});\\ &\text{dilation:} && \boldsymbol{\delta}(\boldsymbol{r}) = A\boldsymbol{r}. \end{aligned}\right\} \tag{A 19}$$

For translations, (A 18) immediately gives $\mathscr{H}'_{ij} = 0$. For rotations, $\nabla\cdot\boldsymbol{\delta} = 0$ and the terms in braces in (A 18) become

$$\{\nabla\psi_i\cdot(\nabla\psi_j\cdot\nabla)+\nabla\psi_j\cdot(\nabla\psi_i\cdot\nabla)\}\,\boldsymbol{\Omega}\times\boldsymbol{r} = \nabla\psi_i\cdot(\boldsymbol{\Omega}\times\nabla\psi_j) + \nabla\psi_j\cdot(\boldsymbol{\Omega}\times\nabla\psi_i) = 0, \tag{A 20}$$

so that $\mathscr{H}'_{ij} = 0$. In conjunction with (32), these results confirm that the degenerate level at E^* is neither split nor shifted by translations or rotations. The vanishing of diagonal elements $i = j$ also confirms that a non-degenerate level is not shifted by these operations.

For dilations, (A 19) gives $\nabla\cdot A\boldsymbol{r} = 2A$ and use of $\nabla\psi\cdot\nabla\boldsymbol{r} = \nabla\psi$ shows that all terms in (A 18) cancel except the first, which gives

$$\mathscr{H}'_{ij} = -2Ak^2\iint_{\mathscr{A}} \mathrm{d}\boldsymbol{r}\,\psi_i\psi_j = -2Ak^2\delta_{ij}. \tag{A 21}$$

Inspection of (32) shows that dilation does not split a degenerate level k^*, but shifts it by

$$k^2 - k^{*2} = -2Ak^{*2}. \tag{A 22}$$

A non-degenerate level is shifted by the same amount. This is precisely the shift expected by virtue of the fact that k scales with area as $\mathscr{A}^{-1}$ and area scales with dilation A as $(1+A)^2$.

The dilation shift (A 21) together with (A 14) gives the normalization condition for any state in terms of its boundary normal derivative:

$$\tfrac{1}{2}\oint \mathrm{d}s\,\boldsymbol{n}(s)\cdot\boldsymbol{r}(s)\,u_i^2(s) = k_i^2 \tag{A 23}$$

(the origin of $\boldsymbol{r}$ is immaterial; this apparent arbitrariness may be reduced by, for example, choosing as origin a boundary point s' and averaging over s').

Finally, we remark that for certain deformations (those for which the new B is not contained entirely within the old), the states defined by (1) do not form a complete set; it is necessary to augment them with states satisfying Neumann boundary conditions. In lowest order, however, these new states do not contribute to the shift or splitting of degenerate levels.